

Transforming the Use of Earth Observation Data: Exascale Training of a Generative Compression Model with Historical Priors for up to 10,000× Data Reduction

Jinxiao Zhang^{2*}, Runmin Dong^{3*†}, Xiyong Wu^{1*}, Xihan Huang¹, Shenggan Cheng⁴, Yunkai Yang³, Zheng Zhou¹, Yunpu Xu¹, Zhaoyang Luo¹, Miao Yang², Fan Wei², Mengxuan Chen², Yang You⁴, Juepeng Zheng³, Weijia Li¹, Yutong Lu^{3,5}, Haohuan Fu^{1,2,5†}

¹Institute of Data and Information, Tsinghua Shenzhen International Graduate School

²Department of Earth System Science, Tsinghua University ³Sun Yat-Sen University

⁴National University of Singapore ⁵National Supercomputing Center in Shenzhen

*Equal contribution, †Corresponding authors.

Abstract

Earth observation is becoming one of the largest data-producing activities in science, yet current pipelines still treat compression as a storage and transmission tool rather than a new way to use data. We present a generative compression framework that learns from historical Earth observation archives and enables on-demand 100× to 10,000× data reduction across downstream tasks. Unlike general visual data, Earth observation repeatedly measures the same evolving planet, making historical-prior learning feasible for extreme compression. To realize this paradigm, we train large generative compression models at exascale on the LineShine Armv9 CPU supercomputer, with co-optimization across model design, kernels, memory hierarchy, runtime, and parallelism. Our implementation sustains 1.54 EFLOP/s and peaks at 2.16 EFLOP/s in end-to-end training. This work shows that historical-prior generative compression can turn Earth observation data into an active, task-adaptive foundation for acquisition, delivery, storage, and scientific use.

Keywords

Image compression, satellite imagery, large-scale training

1 Justification for ACM Gordon Bell Prize

We realize the first exascale training system for historical-prior generative compression of Earth observation data, sustaining 1.54 EFLOP/s and peaking at 2.16 EFLOP/s. Beyond compression itself, this work establishes a new foundation for how Earth observation data are encoded, delivered, stored, and used across

2 Performance Attributes

Attributes	Contents
Category achievement type	<i>Scalability, Time-to-solution, Peak performance, Throughput</i>
Type of method used	<i>Dense Transformer Model</i>
Results reported	<i>Whole application including I/O</i>
Precision reported	<i>BFloat16</i>
System scale	<i>Measured on full-scale system</i>
Measurement mechanism	<i>Timer, FLOP counts</i>

Conference'26, USA

2026. ACM ISBN 978-1-4503-XXXX-X/2018/06

<https://doi.org/10.1145/nnnnnnn.nnnnnnn>

3 Overview of the Problem

Over the past half century, Earth observation has transformed humanity's long effort to observe and understand the Earth into one of the largest and longest-running scientific projects ever focused on a single evolving system.¹ Multi-generational satellite programs such as Landsat and Sentinel have created a vast observational archive across time, scale, modality, and geography [7, 40]. This extraordinary data wealth should enable scientists to study climate change, ecological dynamics, and coastline evolution in new ways. Yet the scale of the archive has made its scientific use increasingly prohibitive: major Earth observation archives now already span hundreds of petabytes [9, 27], and for many important problems, the data that must be accessed, moved, stored, and repeatedly analyzed have reached the PB scale. As a result, broad use of this information remains a luxury rather than a norm. The bottleneck in Earth observation is therefore shifting from data acquisition to data usability [3]. Addressing this bottleneck would do more than reduce storage or transmission cost; it would create a new, more equitable and platform-like foundation for Earth observation data access, sharing, and scientific innovation [50].

Current Earth observation pipelines remain organized around acquisition, downlink, storage, and distribution, with compression serving mainly as a passive utility for reducing bandwidth and archive cost [20, 45, 50]. This design has supported large-scale data collection, but it does not fundamentally change how data are used: scientists must still retrieve, move, store, and repeatedly process massive raw or lightly compressed datasets before analysis. Turning this pipeline into a fundamentally new mode of data use is difficult for three reasons. First, Earth observation archives are enormous, heterogeneous, and continually growing, spanning multiple decades, sensors, spectral bands, resolutions, and operating modes. Second, many scientific and operational tasks impose stringent fidelity requirements, so aggressive reduction must preserve not only visual structure but also physically meaningful information. Third, making historical archives directly usable through a learned model requires training and maintaining that model over global-scale data, which creates an extreme systems challenge in data

¹This long-standing motivation resonates with classical ideas across civilizations. In the Chinese tradition, it finds an early expression in the *Dao De Jing* (道德经): "Man follows Earth, Earth follows Heaven, Heaven follows the Dao, and the Dao follows nature."

throughput, model scale, and computation. Existing compression methods therefore alleviate parts of the burden, but they do not yet turn Earth observation archives into an active, task-adaptive interface for data access and scientific use.

Recent advances in large language models suggest that large-scale compression can become a pathway to usable knowledge when the underlying data already provide a structured encoding of the world. Natural language is such a medium: it is compositional, cross-scale, and accumulated through generations of human observation. Raw visual data, by contrast, generally do not admit such direct large-scale compression into a unified model, because pixel space is far less structured and has much higher effective degrees of freedom. Earth observation may represent a rare exception. Unlike arbitrary visual streams, it repeatedly measures the same evolving planet over decades, yielding strong regularities across geography, seasonality, surface structure, and multispectral response [3]. As a result, global Earth observation archives are not merely massive collections of images, but a historical record of one persistent evolving system observed from many sensors and scales. This makes it plausible to ask whether historical Earth observation data can be compressed into a generative model that does not simply reconstruct pixels, but serves as a learned, task-adaptive prior for how the Earth is queried and used, rather than only as passive reference information [8].

Motivated by this perspective, we develop a historical-prior generative compression framework for Earth observation data. Rather than using compression only to reduce storage and transmission cost, our approach trains a large generative model on global historical archives so that long-term geographic and spatiotemporal priors become directly usable for task-adaptive data reduction. This enables a new mode of interaction with Earth observation data, in which users need not rely exclusively on raw PB-scale archives, but can instead access model-mediated representations matched to different downstream objectives. To make this paradigm practical, we combine large-scale archive construction, generative model design, and exascale training on the LineShine Armv9 CPU supercomputer. The resulting system supports on-demand up to 10,000× data reduction while reframing how Earth observation data can be encoded, delivered, stored, and used.

4 Current State of The Art

The state of the art can be examined along three connected dimensions. First, existing compression methods for Earth observation define the boundary of what can be recovered from the current observation and its transmitted bitstream. Second, recent remote sensing foundation models show that global historical EO archives can support the learning of strong priors, but not yet in a form tailored to extreme-bitrate recovery. Third, large-scale AI training practice shows what system performance is possible at scale, while leaving open the question of how to make this particular workload practical on an emerging CPU supercomputer. Taken together, these three dimensions reveal a common gap: the field still lacks an exascale-trained framework that turns global historical EO priors into a practical capability for task-adaptive compression recovery with a ratio at the scale of several orders of magnitude.

4.1 Compression Methods for Earth Observation

Compression is essential for reducing the storage and transmission cost of large-scale Earth observation data. Existing methods, ranging from standardized codecs such as CCSDS [4] and JPEG2000 [11] to video-based adaptations built on HEVC [28] and VVC [30], have steadily improved coding efficiency for operational sensing systems. More recently, learned compression has further advanced rate-distortion performance by modeling image statistics and redundancy more effectively [1, 25]. Yet these methods still largely share the same basic formulation: they encode the current image and then attempt to reconstruct that same image mainly from the information retained in the transmitted bitstream.

At moderate bitrates, this formulation is often sufficient. In the ultra-low-bit-rate regime, however, the preserved signal becomes too limited to support faithful recovery from the bitstream alone. For Earth observation data, the resulting degradation is not only reflected in lower reconstruction quality or blurred textures, but more importantly in the loss of sensor-related physical characteristics, including spectral signatures, fine spatial structures, and cross-band relationships that are critical for downstream scientific analysis. In this regime, the central bottleneck is no longer only coding efficiency, but whether reconstruction can be supported by priors that extend well beyond the current observation.

This limitation has motivated the emergence of generative compression. In natural images, HiFiC [24] and later diffusion-based methods such as CDC [43] show that, at very low bitrates, high-quality recovery increasingly depends on combining compact representations with strong learned priors. Several recent remote sensing studies have begun to move in this direction. Earth+ [8] uses historical observations in a reference-assisted transmission framework, while MAGC [44] and COSMIC [49] explore generative reconstruction for remote sensing imagery. However, these methods still mainly recover the target from the current image plus limited nearby reference information, or focus primarily on RGB imagery. The current state of the art therefore still lacks a framework that treats global historical EO archives themselves as the primary prior source for ultra-low-bit-rate multispectral recovery.

4.2 Global-Scale Remote Sensing Foundation Models

Recent advances in remote sensing foundation models suggest that large-scale historical EO archives can indeed support the learning of strong priors. Existing efforts already cover a broad spectrum, including spectral modeling, global time-series pretraining, multi-sensor representation learning, multimodal spatio-temporal modeling, and language-conditioned EO generation, as represented by SpectralGPT [14], Prithvi-EO-2.0 [36], DOFA [42], SkySense V2 [48], OlmoEarth [13], Text2Earth [22], and RingMoE [2]. Meanwhile, recent generative models such as MetaEarth [46] and TerraMind [15] further suggest that these large-scale priors can be extended beyond representation learning toward global-scale image generation and multimodal generative modeling.

Functionally, existing works can still be broadly grouped into two categories. The first consists of representation-oriented models, which mainly support understanding tasks such as classification, segmentation, and change detection by learning transferable EO representations from large archives. The second consists of generative models, which explore image generation, text- or multimodal-conditioned generation, and related EO completion tasks. Compact instruction-following vision-language extensions such as TinyRS-R1 [18] further broaden this landscape toward more general EO reasoning, but they are oriented more toward recognition and reasoning than toward recovery or reconstruction.

What these works establish is feasibility, not yet the specific capability required in this paper. They show that global historical EO archives can support strong prior learning, but they do not yet turn those priors into a framework for recovering a specific target observation under an extreme bitrate constraint from the small amount of information retained after compression. In other words, they demonstrate that global EO priors are learnable, but not yet that they are usable for compression-conditioned recovery.

Moreover, many recent EO foundation models span platforms or modalities through platform-aware branches, expert modules, or other modality-specific adaptation paths, as seen in DOFA, SkySense V2, OlmoEarth, and RingMoE. This is a sensible response to EO heterogeneity, but when the objective shifts to global-scale, multi-platform, multispectral compression recovery, it also implies substantial costs in training, storage, updating, and deployment. The state of the art therefore suggests that global prior modeling is possible, while still leaving open how to organize those priors into a practical, scalable framework for ultra-low-bitrate recovery.

4.3 Large-Scale Training Practice and Optimization

Recent large-scale AI training studies, summarized in Table 1, show that high sustained performance at scale depends on more than simply increasing parallelism. Across modern GPU and TPU systems, efficient training increasingly relies on the joint design of parallelization strategy, memory management, communication scheduling, and runtime execution. Frameworks such as Megatron-LM [31], Megatron-DeepSpeed [29], and AxoNN [32] illustrate how hybrid parallelism and memory-aware training can improve throughput and scalability, while systems such as MegaScale [17] further highlight the importance of runtime robustness and system-level coordination in long-running jobs at extreme scale. Table 1 also shows that, although remote sensing foundation models are beginning to reach substantial scale, their reported training system characteristics remain far less explored than those of frontier language and scientific AI workloads.

However, the workload studied in this paper is not simply another instance of frontier model training. It combines global historical archive ingestion, large generative modeling, long visual sequences, multispectral physical constraints, and ultra-low-bitrate recovery objectives in a single system problem. Existing state-of-the-art results are therefore highly informative as performance references, but they do not directly resolve the challenge of making this workload practical. That challenge becomes even sharper on

an emerging Armv9 CPU supercomputer, where many accelerator-oriented training recipes cannot be applied directly. In our setting, efficient execution is further constrained by limited SME utilization, higher runtime overhead, hierarchical HBM/DDR memory, and the interaction of multiple system factors that prevent the training stack from reaching high performance. The remaining gap is thus not only whether exascale training is possible, but whether this particular Earth observation workload can be trained efficiently enough to make global historical priors operational.

5 Target Platform and Architectural Challenges: The Armv9-Based LineShine Supercomputer

5.1 System Architecture

The LineShine supercomputer at the National Supercomputing Center in Shenzhen (NSCC-SZ) is an exascale HPC-AI converged system built on Armv9-based LX2 processors and interconnected by the LingQi high-speed network (LQLink) with 1.6 Tb/s per node.

As shown in Figure 1, each compute node contains two LX2 processors. Each processor integrates two compute dies and 304 CPU cores, organized into eight CPU clusters with 38 cores per cluster. Each core has a 32 KB L1 instruction cache and a 32 KB L1 data cache, while each cluster shares a 28.5 MB L2 cache.

LX2 adopts a hierarchical memory system that combines high bandwidth with large capacity. Each processor provides 32 GB on-package HBM with 4 TB/s peak aggregate bandwidth, together with 256 GB off-package DDR. Each die contains four cluster-local HBM domains and four DDR domains, giving 16 NUMA domains per processor. In this design, each cluster is associated with one HBM domain and one DDR domain. HBM access is strongly locality-sensitive, while DDR access is more uniform within a die but shared across multiple clusters. Each die also includes a dedicated SDMA engine for DDR-HBM data movement.

For computation, LX2 supports both Armv9 SVE and SME. SVE enables vector execution, while SME provides matrix acceleration through ZA tile registers and outer-product instructions, making it particularly effective for dense kernels such as GEMM. A single LX2 processor delivers a theoretical peak of 60.3 TFLOP/s in Float64, 240 TFLOP/s in BFloat16/Float16, and 960 TOP/s in INT8.

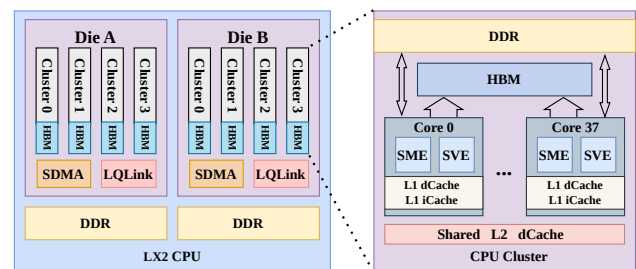


Figure 1: Architectural overview of the LX2 processor.

Table 1: State of the Art Training Practices on Massively Parallel Supercomputer. MFU for Model FLOPs Utilization.

Application	Field	Model Size	Batch Size	Hardware	Scale	MFU	Sustained PFLOP/s
Narayanan et al. [26]	Language	1000 B	6.3 M	NVIDIA A100	3,072 GPUs	52%	502
MT-NLG [34]	Language	530 B	4.0 M	NVIDIA A100	3,360 GPUs	36%	379.7
MegaScale [17]	Language	175 B	12.5 M	NVIDIA A100	12,288 GPUs	55%	2166.3
Dash et al. [5]	Language	1000 B	19.7 M	AMD MI250X	2,048 GPUs	31.9%	188.0
AxoNN [33]	Language	60 B	16.8 M	NVIDIA H100	6,144 GPUs	23%	1423.1
MProt-DPO [6]	Protein Design	3.5 B	4.9 M	Intel Max 1550	38,400 GPUs	45.5%	4110*
ORBIT-2 [39]	Climate	10 B	671 M	AMD MI250X	65,536 GPUs	~16%	4100
Tabuchi et al. [37]	Cosmology	7 M	4 K	Fujitsu A64FX	16384 CPUs	~2.0%	~2.22
SkySense V2 [48]	Remote Sensing	0.67 B	4 M	NVIDIA H20	128 GPUs	/	/
Prithvi-EO-2.0 [36]	Remote Sensing	0.6 B	4 M	NVIDIA A100	240 GPUs	/	/
OlmoEarth [13]	Remote Sensing	0.3 B	150 K	NVIDIA B200	/	/	/
RingMoE [2]	Remote Sensing	14.7 B	/	Ascend 910	512 NPUs	/	/
D2AR (This work)	Remote Sensing	6.3 B	252 M	Armv9 LX2 CPU	40,960 CPUs	15.7%	1543

* RL training (DPO); reference model inference only, with no gradients or backpropagation. The two rows highlighted in grey represent works that rely on large-scale training on CPU platforms.

5.2 Challenges and Opportunities

Although LX2 offers strong compute capability and memory bandwidth, achieving efficient large-scale training on the LineShine supercomputer remains challenging.

The first challenge is the limited local memory available for training states. In large-scale training, parameters, activations, gradients, and optimizer states cannot be kept entirely within the memory resources local to a single cluster. On LX2 CPU, each cluster is associated with 4 GB HBM and 32 GB DDR, which is far from sufficient for the full working set of modern large-scale training. They must therefore be distributed across clusters, with DDR serving as the main storage space. This makes the organization of training states a basic requirement for execution and an important factor in later data access and communication cost.

The second challenge is the lack of an efficient software stack for large-scale CPU training. Existing deep learning frameworks and runtime systems are largely optimized for GPU platforms, where high-throughput kernels help amortize launch and scheduling overheads. On CPU platforms, these overheads become much more visible. Operator dispatch, runtime scheduling, tensor management, and synchronization can all take a non-negligible fraction of execution time. Efficient communication support for large-scale CPU training is also limited. Existing communication libraries are not well tuned for this setting, especially for BFloat16 communication, topology-aware collectives, and fine-grained overlap between communication and computation. As a result, communication overhead remains a major barrier to high sustained performance on LineShine.

Another challenge is topology-sensitive memory access. HBM delivers high bandwidth only when accessed locally. In our measurements, local HBM bandwidth reaches 450 GB/s, but drops to 230 GB/s for same-die remote access, 170 GB/s across dies, and 45 GB/s across CPUs. DDR bandwidth is more stable within a die, but still decreases from 125 GB/s locally to 110 GB/s across dies and 45 GB/s across CPUs. This behavior makes locality-aware data placement essential rather than optional.

The final challenge is kernel efficiency. While SME offers high peak throughput for matrix operators, sustaining that performance requires coordinated control of data layout, cache residency, memory movement, and kernel granularity. Training introduces frequent tensor reshaping, irregular memory access, and short-lived kernel execution, all of which can leave the matrix units underutilized if the runtime is not carefully co-designed.

Taken together, these challenges point to four key optimization opportunities on LineShine: parallel design for distributed training states, framework and communication support tailored for large-scale CPU training, locality-aware use of hierarchical HBM and DDR memory, and SME-oriented kernel and runtime co-design for high sustained efficiency.

6 Innovations Realized

6.1 Overview

This work introduces an integrated solution for global-scale Earth observation data compression and reconstruction from three tightly connected perspectives, as shown in Figure 2. At the framework level, we reorganize how data are compressed, delivered, and reconstructed for use. At the model level, we turn massive historical archives into controllable reconstruction capability. At the system level, we make this training paradigm practical on an exascale Armv9 CPU platform.

6.2 Framework-Level Innovations

The primary motivation for our redesign stems from the extreme imbalance between the scale of Earth observation archives and the practicality of using them. To process global-scale data while maintaining physical fidelity, conventional monolithic pipelines face severe computational bottlenecks. At the same time, the heterogeneity of multi-source satellite platforms leads to non-standardized execution flows and massive I/O overhead. We propose a Dual-Decoupled Asymmetric Compression and Reconstruction (D2AR)

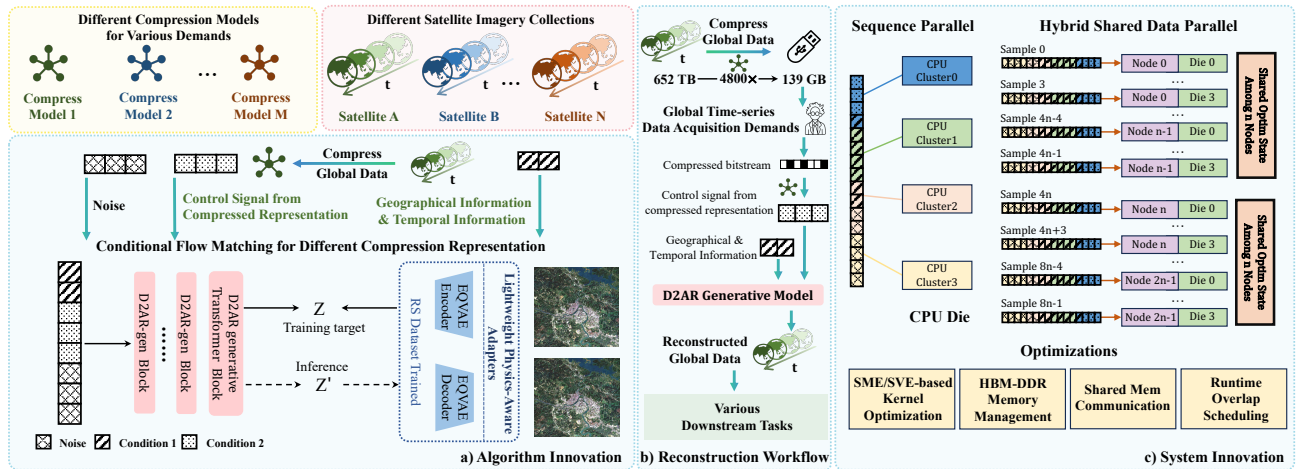


Figure 2: Overview of the proposed historical-prior generative compression framework for Earth observation. (a) Algorithm design for compressing global historical archives into generative priors with geographic and temporal conditioning. (b) Reconstruction workflow for on-demand recovery from compressed representations for downstream use. (c) System design for exascale training on the LineShine Armv9 CPU supercomputer.

framework that addresses this challenge at the system level by fundamentally reorganizing the coupling among compression, reconstruction, and user access. By doing so, it turns a fragmented scientific workflow into a structured computation-and-service pipeline that can simultaneously support extreme compression, flexible reconstruction, and downstream scientific use.

6.2.1 Task Decoupling and Asymmetric Space-Ground Computation.

To eliminate the inefficiency of training independent models for specific compression ratios and modalities, D2AR introduces a systemic task decoupling. The workflow is divided into two highly specialized execution stages. In the on orbit stage, the lightweight frontend D2AR-comp flexibly utilizes arbitrary existing compression models to transform diverse remote sensing inputs into a highly compressed intermediate bitstream. This bitstream is then processed by a lightweight pretrained feature mapper, which remaps it into control tokens representing the compressed signal. In the ground based stage, rather than treating these tokens as a direct pixel source for traditional decoding, they serve as a conditional control signal to guide D2AR-rec, our core Flow Matching reconstruction model. This profound architectural shift converts a data intensive transmission and decoding bottleneck into a highly homogeneous compute intensive generative task. For D2AR-rec, we adopt a generative model architecture based on Z-Image. Compared to existing generative models such as Stable Diffusion 3 and FLUX, which rely on massive dual stream architectures and incur severe memory bandwidth overheads, the Z-Image architecture utilizes a unified single stream diffusion transformer that significantly reduces parameter redundancy and memory access costs. This allows the ultra low entropy compressed signal to be progressively reconstructed with high fidelity within a model that encapsulates the global historical data priors of the specific sensor platform. Therefore, the supercomputer can concentrate its peak capability on a unified reconstruction logic while seamlessly supporting flexible on demand operations across extreme compression ratios.

6.2.2 User-Centric Reconstruction Workflow. This framework-level decoupling also changes how scientists interact with Earth observation data in practice. Instead of forcing users to acquire, move, and locally manage massive raw archives, supercomputing centers can expose compressed observation information at multiple precision levels as a new data service layer. Researchers then select the compression level most appropriate for their scientific target and invoke the corresponding D2AR-rec model for reconstruction and analysis. Empirically, Table 3 demonstrates that this framework achieves substantial improvements in high fidelity reconstruction over existing compression paradigms across extreme compression scenarios at magnitudes ranging from thousands to tens of thousands of times. Furthermore, Table 5 proves that thousandfold compression incurs negligible accuracy degradation in downstream land cover scene classification tasks, while ten thousandfold compression results in only a marginal performance drop of approximately 1% in both F1 score and mean average precision. In this workflow, storage, transfer, and reconstruction are no longer fixed upstream decisions; they become configurable elements of data use itself. This is the practical mechanism through which D2AR turns extreme compression into a new paradigm for accessing and using Earth observation data.

6.3 Model-Level Innovations

At the model level, D2AR separates sensor-specific physical heterogeneity from the core generative learning problem, while injecting global historical knowledge directly into the reconstruction path. This combination allows a unified reconstruction backbone to operate across multiple observation settings, effectively preserving physical consistency while maintaining a robust capability to recover information degraded under extreme compression.

6.3.1 Physical Decoupling and Standardized Generative Backbone. Recognizing the intrinsic physical heterogeneity of Earth observation sensors, D2AR implements a modular physical decoupling strategy. We use pre-trained EQ-VAE [19] encoders and decoders as lightweight physics-aware adapters. The unique imaging physics and spectral characteristics of specific sensors, such as synthetic aperture radar or multispectral platforms, are encapsulated within these adapters. Crucially, the optimization objective of D2AR-rec is not to reconstruct pixel-level images directly, but to generate the structured latent space produced by the EQ-VAE encoder. By executing Flow Matching [21] within this latent domain, we decouple complex physical restoration from the core generative process. Once latent reconstruction is complete, the corresponding EQ-VAE decoder maps the result back to the original physical space. This design keeps the primary computational workload, namely the core backbone of D2AR-rec, standardized and platform-agnostic. By isolating platform-dependent physics in modular adapters, we establish a consistent execution flow across modalities and enable unified optimization of memory access patterns and communication kernels on exascale supercomputing nodes.

6.3.2 Prior-Driven Reconstruction and Global Information Recovery. To push beyond the theoretical reconstruction boundaries imposed by extreme compression ratios, D2AR-rec introduces a global geographic prior injection mechanism that transforms massive historical observation archives into actionable reconstruction capability. We encode global spatiotemporal priors into continuous geographic embeddings and dynamically inject them into the latent Flow Matching process as a global control. This establishes a deep semantic linkage between the current compressed observation and the global information accumulated by the corresponding sensor platforms. By leveraging this shared global context, the model can effectively compensate for the structural and spectral high frequency information that is lost during extreme compression. Empirically, Table 4 validates the effectiveness of the performance improvements achieved by scaling up the global data learning size. This joint global and local control strategy substantially unleashes the utility of massive historical datasets, effectively turning the storage capacity and memory bandwidth of the supercomputer into a direct gain in the physical fidelity of reconstructed observations.

6.4 System Innovations

Training large generative models on an emerging Armv9 CPU with hierarchical memory requires more than a conventional GPU-oriented stack. End-to-end efficiency is jointly constrained by three coupled factors: data reuse in SME-based kernels, limited HBM capacity across operators and tensor lifetimes, and the communication-computation balance shaped by system topology.

Our design follows a coordinated, layered approach from kernels to memory to parallelism. First, we develop an SME-oriented GEMM strategy that adapts tiling and buffering to problem geometry and cache limits. Second, we treat HBM as a global placement problem, prioritizing critical tensors under tight capacity constraints. Third, we co-design sequence and hybrid data parallelism with hardware topology to align communication and state placement with the system structure.

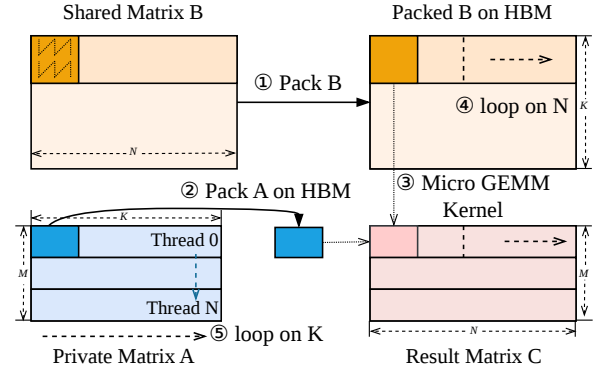


Figure 3: GEMM workflow. Threads cooperatively pack the shared matrix B into HBM. The computation is organized as a tiled loop over the K dimension: each thread packs its local tile of A into HBM, traverses the shared dimension, and performs micro-kernel computations to accumulate results into matrix C.

6.4.1 Reuse-Directed Asymmetric SME-GEMM. On Armv9 CPUs with hierarchical memory, GEMM performance is not only limited by compute power, but also by how well data stays in cache and gets reused. If cache locality is poor, even compute-heavy workloads quickly become memory-bound. To address this, we do not use a single fixed kernel. Instead, we adapt the computation strategy based on the shape of the problem, choosing the approach that maximizes data reuse.

Specifically, we develop two complementary SME micro-kernels, $64 \times K$ by $K \times 16$ and $16 \times K$ by $K \times 64$, and select between them at runtime according to the relative sizes of M and N . This design enables two dual dataflows: one organized around M -major reuse and the other around N -major reuse. In each case, the wide-tile operand is kept thread-private to maximize intra-thread reuse, while the narrow-tile operand is streamed across the computation.

To ensure data stays in cache, we derive the parameter `magic_k` based on how much data can fit in L2 cache, rather than tuning it empirically. We further use reuse-aligned thread partitioning and near-uniform tiling to reduce tail imbalance and synchronization overhead under non-divisible problem sizes. Concretely, the partitioned dimension follows the selected reuse direction, so that threads operate on tiles with stable private reuse and minimized interference.

We further apply asymmetric memory optimizations, as shown in Figure 3. The streamed operand is prefetched and stored in a large HBM buffer to sustain high bandwidth, while the thread-private operand uses only small local buffers without prefetching. For the output matrix, we adopt a K -aware accumulation policy: when $K < \text{magic}_k$, the result is written back directly; otherwise, FP32 partial sums are accumulated in HBM before final write-back. Bias addition and output scaling are fused into the main compute and write-back path to further reduce memory traffic.

Overall, this design treats GEMM optimization as a unified problem of data reuse and locality. Kernel shape, thread mapping, memory layout, and accumulation strategy are all co-designed to maximize cache reuse and minimize memory movement.

6.4.2 Operator- and Lifetime-Aware HBM Strategy. While the SME-GEMM optimization improves the efficiency of core dense computation, overall training performance remains strongly constrained by the limited capacity of on-package HBM. On the target platform, HBM cannot hold all model states and intermediate tensors simultaneously, so its usage must be planned globally rather than assigned uniformly. We therefore formulate HBM placement as a constrained resource-allocation problem: under a fixed capacity budget, HBM should be reserved for tensors whose placement yields the highest end-to-end performance benefit after accounting for both kernel sensitivity and tensor lifetime.

Our strategy is guided by the operator-level characterization in Figure 4. The results show that the benefit of HBM placement is highly non-uniform across operators and execution phases. In the forward pass, the attention operator exhibits the clearest sensitivity to HBM bandwidth, while other operators obtain smaller gains in the context of full-model execution. Based on this observation, we place only the output activations of attention in HBM during the forward pass, while keeping other intermediate tensors in DDR to relieve HBM pressure. This choice concentrates scarce HBM capacity on the most bandwidth-sensitive forward tensors instead of diluting it across all operators. Moreover, because the attention outputs are subsequently cast from float32 to float16, the corresponding HBM allocation can be released immediately after the cast, further reduce the HBM footprint.

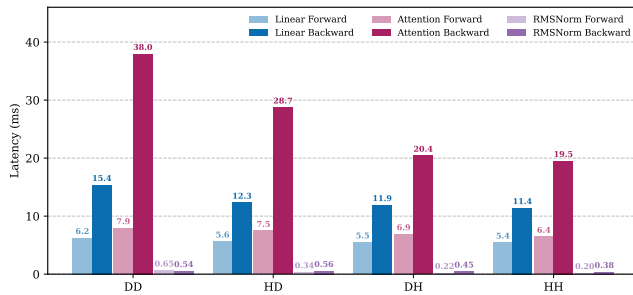


Figure 4: Forward and backward latency of core operators across different memory configurations (ms). H denotes HBM and D denotes DDR. The two-letter column headers indicate the memory placement of input and output tensors, respectively. For instance, HD denotes that input tensor resides in HBM while output tensor is allocated in DDR.

In the backward pass, the situation differs. Backward kernels consistently benefit from HBM, and most gradients and intermediates are short-lived, so we place all backward allocations in HBM. The main exception is parameter gradients, which persist for accumulation and communication. To avoid exhausting HBM, we offload them to DDR during the SP communication phase, freeing space while retaining the benefits of the HBM.

In conclusion, our strategy considers both *operator sensitivity*, which captures the performance gain from using HBM, and *tensor lifetime*, which determines whether this gain is sustainable under limited capacity. This joint design prioritizes HBM for the most critical operators, maximizing overall training throughput.

6.4.3 Asynchronous Runtime and Overlap Execution. To reduce runtime overhead and improve hardware utilization, we design an asynchronous execution runtime. We introduce a dedicated launch thread to overlap framework overheads (e.g., operator dispatch, memory allocation, and tensor view operations) with kernel execution. Our profiling shows that the default PyTorch runtime incurs approximately 24.2% overhead. With the asynchronous runtime, this overhead is reduced to 1.9%, resulting in near-optimal overlap between computation and framework execution. In addition, we implement communication-computation overlap using hook-based scheduling and explicit synchronization mechanisms. All communication operations are overlapped with ongoing computation whenever possible, minimizing idle time and improving overall throughput. Furthermore, we assign dedicated CPU cores to handle communication tasks, reducing interference with computation.

6.4.4 Topology-Aligned Parallelization Strategy. To scale efficiently to full machine, we must carefully design the parallelization strategy that matches the hardware topology, rather than directly adopting a generic distributed design. We therefore use a hierarchical parallelization scheme aligned with the processor structure. Each MPI process is bound to one CPU cluster, which contains 38 cores, with 37 cores available to the application, along with 32 GB DDR and 4 GB HBM. Within a die, four processes in different NUMA domains can communicate through shared memory.

On top of this shared-memory, we apply sequence parallelism (SP) across the four intra-die processes and use ring attention for attention computation. This reduces per-process activation memory and keeps SP communication within the low-latency shared-memory. At a larger scale, we introduce hybrid shared data parallelism (HSDP), which partially shares and shards optimizer states across processes within four nodes. Compared with full replication, this reduces optimizer-state memory and eliminates redundant optimizer computation.

We further optimize communication inside the SP domain. Shared memory is used to accelerate both ring data exchange in attention and gradient all-reduce within the SP group. In addition, we adopt different communication schedules for forward and backward. The forward pass exchanges K and V , while the backward pass exchanges Q and grad_out . Compared with a symmetric design that exchanges K - and V -related tensors throughout backpropagation, this reduces backward communication volume by about 50%.

This design integrates SP and HSDP into a unified hierarchical parallel framework. We further evaluate the impact of SP and HSDP group sizes, as shown in Figure 5. Specifically, we test two sets of configurations: SP= 4 with HSDP= 4/16/32, and HSDP= 16 with SP= 2/4/8. Here, SP×HSDP denotes the total number of shards for each configuration. The results are used to understand the trade-off between SP communication overhead and HSDP memory savings, and to select the final parallel configuration.

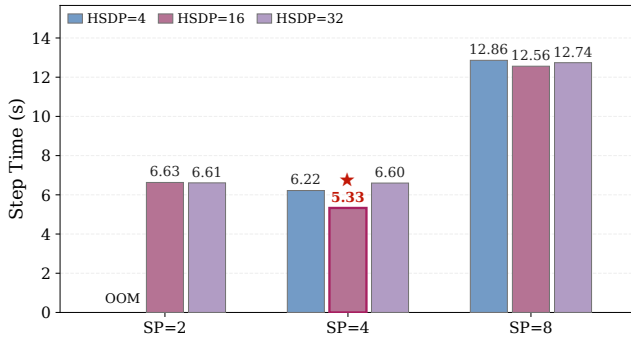


Figure 5: Performance comparison across different parallelism configurations for D2AR-rec-6B on 128 nodes, including Hybrid Shared Data Parallelism (HSDP) and Sequence Parallelism (SP).

7 How Performance was Measured

We use three D2AR-rec model configurations in the performance experiments, namely D2AR-rec-3B, D2AR-rec-6B, and D2AR-rec-8B, as summarized in Table 2.

Table 2: ARCHITECTURAL DETAILS IN THE PERFORMANCE EXPERIMENTS.

Model	Parameters	Layers	Hidden-Size	Heads
D2AR-rec-3B	3B	17	3840	30
D2AR-rec-6B	6B	36	3840	30
D2AR-rec-8B	8B	46	4096	32

We report two complementary performance metrics. The primary metric is the sustained end-to-end BFloat16 FLOP/s over full training iterations, capturing the realized cost of computation, communication, and data movement in actual distributed execution. Alongside this, we report Model FLOPs Utilization (MFU), which quantifies the fraction of the system’s theoretical peak FLOPs that is effectively achieved during training. In addition, we provide a compute-only metric, referred to as Peak FLOPs in the following figures and tables, which is derived solely from forward and backward model computation and excludes communication and I/O overhead.

For each configuration, we run the training loop for twenty iterations with fixed model size, sequence length, and batch configuration, and report the average per-iteration time over the last ten iterations to reduce warmup effects and capture steady-state execution. We follow the analytical FLOP formulation used in Megatron-LM [31] to estimate model computation, and compute sustained BFloat16 FLOP/s by dividing the analytical model FLOPs by the measured end-to-end iteration time. MFU is then defined as the ratio between the measured sustained BFloat16 FLOP/s of the full system and the aggregate theoretical BFloat16 peak of the participating nodes. Since a single LX2 node provides 480 TFLOP/s theoretical BFloat16 peak, all MFU values in this work are normalized against this vendor-advertised theoretical peak rather than an empirically measured GEMM upper bound.

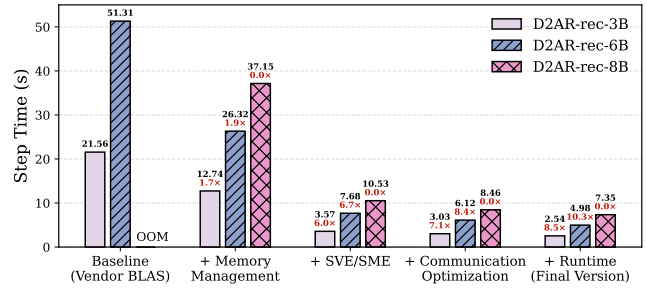


Figure 6: Single-node runtime under different optimization stages across model sizes.

8 Performance Results

We evaluate performance results from three complementary perspectives. First, we quantify how much each optimization contributes on a single node. Second, we test whether these gains are preserved at scale and whether the proposed system can sustain exascale training throughput on the full machine. Third, we validate that the training system supports the intended scientific objective of historical-prior generative compression across extreme compression ratios, global prior utilization, and downstream task utility.

8.1 Single Node

We first study single-node performance to isolate the effect of local optimizations before moving to distributed scaling. Figure 6 reports the runtime under successive optimization stages for three model sizes, D2AR-rec-3B, D2AR-rec-6B, and D2AR-rec-8B.

As shown in Figure 6, the proposed optimizations consistently reduce runtime for all three models. Starting from the vendor-BLAS baseline, introducing the HBM-aware memory strategy already yields a clear reduction in step time, indicating that memory placement is a first-order factor on this hierarchical-memory CPU platform. After further incorporating the optimized SVE/SME kernels, runtime drops more substantially, showing that dense-compute efficiency becomes the dominant lever once the main memory bottleneck is alleviated. Communication optimization and the asynchronous runtime then bring additional gains by reducing exposed communication, launch, and synchronization overhead.

For the 6B model, the runtime is reduced from 51.31 s in the baseline to 26.32 s after HBM-aware memory management, then to 7.68 s with SVE/SME kernel optimization, 6.12 s with communication optimization, and finally 4.98 s with the asynchronous runtime, corresponding to an overall speedup of 10.3 \times . Similar step-wise improvements are observed for the 3B model, whose runtime decreases from 21.56 s to 2.54 s. For the 8B model, the baseline configuration results in an out-of-memory failure, while execution becomes feasible once the memory optimizations are introduced.

8.2 Weak Scaling Performance

8.2.1 Weak Scaling Efficiency. We evaluate weak scaling by proportionally increasing the global workload with the number of

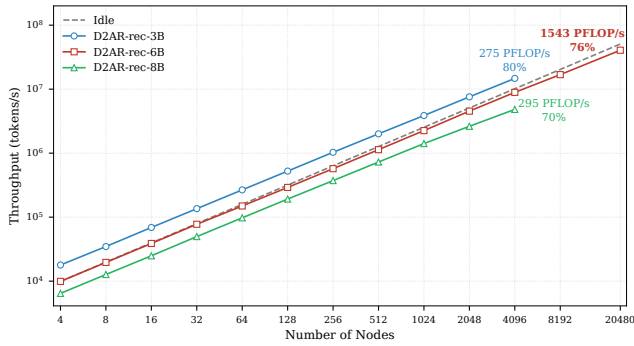


Figure 7: Weak scaling performance of the proposed system for three model sizes. In all cases, the global workload is increased proportionally with the number of nodes while keeping the per-node workload fixed.

nodes while keeping the per-node workload fixed. Figure 7 reports the results for three model sizes: 3B model from 1 to 4096 nodes, 6B model from 1 to 20480 nodes, and 8B model from 1 to 4096 nodes.

Overall, all three configurations exhibit good weak scaling behavior. The 6B model delivers the main large-scale result, sustaining 1.54 EFLOP/s at 20480 nodes with a weak scaling efficiency of 76.0%, demonstrating that the proposed system remains effective even at full-machine scale. Under this configuration, the corresponding Peak FLOPs reaches 2.16 EFLOP/s. For the 3B and 8B models, the system scales to 4096 nodes and achieves 275 PFLOP/s and 295 PFLOP/s sustained performance, with corresponding weak scaling efficiencies of 80.4% and 70.4%, respectively.

8.2.2 Full-Scale Training Scenario. Unlike strong scaling, where more nodes are used to reduce the iteration time of a fixed small problem, our goal is to continuously incorporate larger portions of the global historical archive while keeping the per-node workload, optimizer behavior, and memory footprint stable. In this regime, additional nodes increase total training throughput and global batch size, so that larger machine scale translates into broader archive coverage rather than simply faster processing of a fixed dataset fragment.

This distinction is especially important for historical-prior generative compression. A single epoch over global Earth observation archives is already a massive computational task, and the model’s scientific value depends on exposure to broader geographic and temporal coverage. Accordingly, the key full-machine question is not whether a fixed task can be further accelerated, but whether training remains efficient as the global workload grows with machine size. Figure 7 shows that this is indeed the case, with the proposed system maintaining 76% weak-scaling efficiency at 20480 nodes. More importantly, full-scale training improves not only system throughput but also optimization. Starting from the same pre-trained checkpoint and continuing training on global Earth observation data, the full-machine large-batch setting reaches the same intermediate loss level in only 50 steps, whereas the 4-node configuration still does not reach that level after more than 5000 steps.

The large-batch trajectory is also smoother, with smaller loss oscillations throughout training. Together, these results show that the exascale machine is not used merely to accelerate a conventional training recipe, but to enable a different training regime in which the model can ingest more of the Earth, more efficiently and more stably, to build the desired historical prior.

8.3 Application-Level Validation

8.3.1 Generalization for Different Compression Ratios. To evaluate the flexibility and robustness of this paradigm, we evaluate three cases using distinct compression baselines: HL-CompNet [41] (Case 1), LIC-TCM [23] (Case 2), and MLC++ [16] (Case 3), spanning compression ratios from 6000× to 18,000×. Using Sentinel-2 multispectral imagery as a benchmark, we conduct ablation studies across eight consecutive years of data from the global top-1,000 cities. Table 3 shows that the generative reconstruction model consistently outperforms signal-only recovery baselines across all tested compression regimes. The gains are especially clear on perceptual and structural metrics such as LPIPS and MS-SSIM, while also improving or preserving physically relevant indicators such as NDVI error. These results validate that the decoupled framework remains effective across diverse and extreme operating points rather than only at a single bitrate.

Table 3: Reconstruction Performance Across Different Compression Ratios.

Method	Comp. Ratio	PSNR↑	LPIPS↓	MS-SSIM↑	NDVI↓
Case 1 [41]	6104	13.2252	0.6497	0.5922	0.0982
+D2AR-rec (Ours)	6104	14.9484	0.1074	0.9238	0.0915
Case 2 [23]	6295	15.3820	0.4504	0.9087	0.0776
+D2AR-rec (Ours)	6295	16.5998	0.1218	0.9537	0.0818
Case 3 [16]	17777	13.1023	0.6189	0.8416	0.0978
+D2AR-rec (Ours)	17777	14.1299	0.1193	0.9018	0.0893

8.3.2 The Necessity of Utilizing Global Data. To verify the necessity of comprehensive global data for effective prior learning, we conduct a comparative study focused on the density of spatial priors. We partition the dataset from 1,000 representative global cities into distinct configurations to observe the impact of geographic coverage on reconstruction fidelity. The control group uses the full extent of the 1,000 cities over a six-year period for training, while the experimental group intentionally restricts the spatial coverage to 900 cities over the same duration. Both models are evaluated on a held-out validation set comprising the remaining 100 cities during the subsequent two-year period. As shown in Table 4, the model trained on the full geographic extent consistently outperforms the spatially restricted counterpart. This gap confirms that the generative recovery process is sensitive to the completeness of the global prior: adding the remaining 100 cities provides geographic context that improves generalization to unseen temporal intervals in those regions. These findings support a central claim of the paper, namely that using the full scale of global historical archives is not a mere data expansion, but a direct source of reconstruction capability.

Table 4: Ablation Study Validating the Performance Gains from Expanding Global Prior Coverage.

Data Scale	PSNR \uparrow	LPIPS \downarrow	MS-SSIM \uparrow	NDVI \downarrow
900 Cities	12.1516	0.3273	0.8474	0.0934
1000 Cities	12.4708	0.2990	0.8586	0.0906

8.3.3 Downstream Utility. To verify the practical value of extreme compression for downstream analysis, we conduct validation on a representative land-cover scene classification task using the DynamicEarthNet [38] Sentinel-2 dataset, which contains 896 images with corresponding 7-class land-cover labels. Using the same dataset split, we establish strictly paired evaluation pipelines. For each compression baseline including HL-CompNet, LIC-TCM, and MLC⁺⁺, we train a ResNet 18 [12] model exclusively on the reconstructed data and compare it against a corresponding ResNet 18 baseline independently trained on the original data. We report Exact Accuracy [47], Macro F1-Score [35], and mean Average Precision (mAP) [10]. Exact Accuracy is a strict instance-level metric that counts a prediction as correct only when the entire multi-label vector matches the ground truth.

As shown in Table 5, the downstream classification performance on reconstructed data exhibits only limited degradation even under extreme compression. Across the tested settings, Macro F1 remains unchanged or changes only marginally, while mAP remains close to the original-data baseline. These results indicate that the proposed reconstruction pipeline preserves a substantial fraction of the semantic and structural information required by downstream tasks, rather than optimizing only for pixel-level fidelity.

Table 5: Downstream task evaluation on the land cover scene classification.

Method	Case 1 + D2AR-rec		Case 2 + D2AR-rec		Case 3 + D2AR-rec	
	Original	Ours	Original	Ours	Original	Ours
Exact Acc	0.5000	0.4792	0.4688	0.5000	0.5000	0.4792
Macro F1	0.7540	0.7540	0.7540	0.7540	0.7540	0.7547
mAP	0.8535	0.8465	0.8761	0.8372	0.8535	0.8312

8.3.4 Global Compression and Reconstruction Application. Taking the global thousandfold compression of Sentinel 2 data as an example, Figure 8 (a) visualizes the relative gains of the lossy paradigm over traditional lossless methods. The spatial distribution reveals significantly higher compression gains in dense urban areas. Since high intrinsic information entropy renders lossless algorithms largely ineffective, the deep entropy reduction of the lossy frontend maximizes efficiency while severely exacerbating reconstruction challenges. This firmly validates the necessity of introducing a global prior driven generative model to synthesize discarded details.

Figure 8 (b) evaluates the visual reconstruction and Figure 8 (c) shows the corresponding spectral curves across hundredfold to ten thousandfold compression scales. At hundredfold compression, D2AR delivers high fidelity reconstruction with highly consistent

visual textures. Under extreme ten thousandfold compression, although micro textures are inevitably smoothed, the model successfully maintains the macroscopic semantic layout. Crucially, global physical priors effectively maintain the structural integrity of the spectral curves, ensuring high reliability for downstream quantitative analyses despite extreme information loss.

9 Implications

Continuous Earth observation is essential for addressing global challenges, yet sensing capabilities now vastly outpace downlink and storage capacities. Current pipelines treat each acquisition as an isolated file, ignoring the immense spatiotemporal redundancies of repeatedly measuring the same evolving planet. To resolve this bottleneck, our work suggests moving beyond merely building better codecs or larger archives by fundamentally redefining the role of historical data itself. Specifically, we demonstrate that global historical archives can be condensed into actionable generative priors. Activated by ultra-low-bitrate features, these priors recover physical information absent from the transmitted signal. This transforms compression from a passive storage utility into an active mechanism for data utilization. In this paradigm, accumulated prior knowledge becomes as critical as transmitted bits, fundamentally allowing ground-based compute and historical knowledge to be systematically traded for satellite-to-ground bandwidth, storage footprint, and data accessibility.

This shift has implications across the full Earth observation ecosystem. On satellites, for platforms with sufficient onboard compute, the role of transmission can move from pixel-by-pixel relay toward task-adaptive feature export, quality-aware filtering, and progressive information release. At ground stations, reception can evolve from simple data ingress into the first scheduling layer of a space-ground computing continuum, where streams are routed according to latency, importance, and reconstruction objectives. At the level of the largest centralized archives, supercomputing data centers can transition from passive warehouses into generative prior engines that continuously absorb global history, update reconstruction models, and serve feature-based access at scale. At regional or institutional data centers, the same paradigm enables task-specific reconstruction, local adaptation, and selective caching without requiring full replication of petabyte-scale raw archives. For end users, especially those outside elite storage environments, access can gradually shift from downloading massive physical files toward obtaining compact features, derived products, or on-demand reconstructions matched to specific scientific tolerances. In this sense, the paradigm has the potential to restructure the entire data ecology of Earth science, from onboard acquisition to personal scientific use. Importantly, this is not a purely hypothetical direction: onboard AI missions have already begun filtering or compressing imagery before downlink, while major Earth observation platforms are increasingly combining archive access with cloud-side processing close to the data.

The system implications are equally important. Condensing long-term global observation information into computational priors is not only a modeling problem but also an infrastructure problem dominated by data ingestion, preprocessing, scheduling, storage

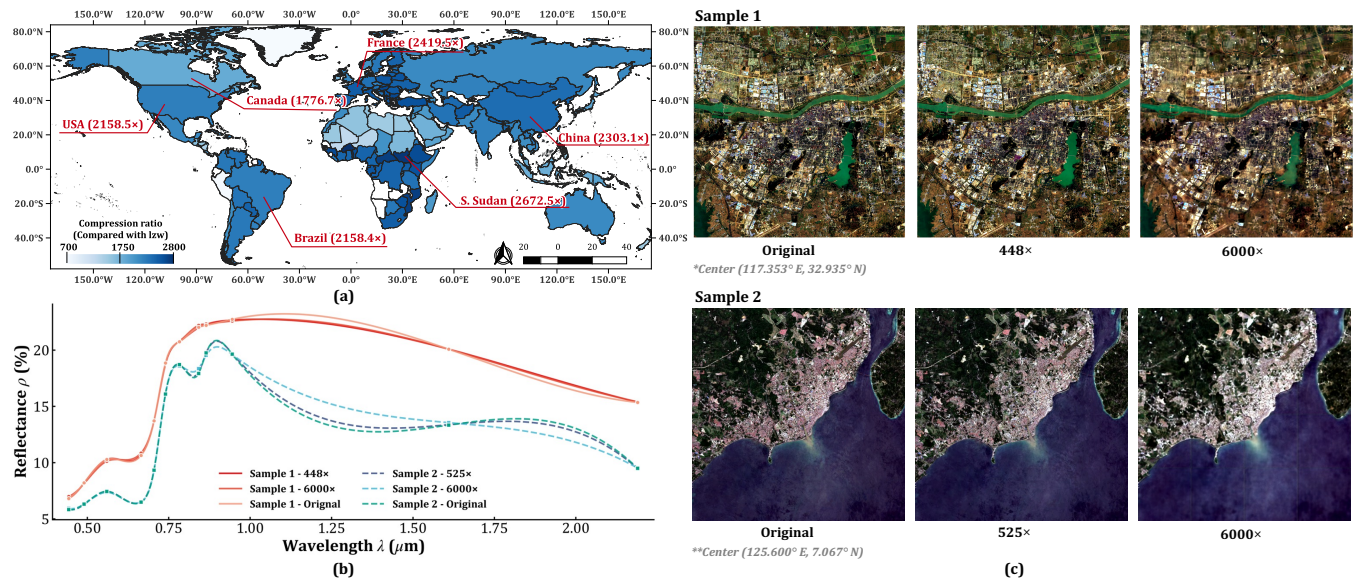


Figure 8: Visual Comparison under different compression ratios and corresponding spectral curves.

access, and distributed runtime efficiency. Our results therefore provide evidence that CPU-centered supercomputers, and Arm platforms in particular, can serve as highly effective substrates for large-scale scientific AI. Beyond raw dense computation, such systems offer natural advantages for the control-heavy and data-intensive parts of the workload, including complex preprocessing, distributed input/output orchestration, memory management, communication scheduling, and coupling with large storage systems. These properties are especially relevant for emerging hybrid scenarios in which model training, retrieval, simulation, tool use, and agent-like runtime logic coexist within the same AI-for-Science pipeline.

Another implication is methodological. The physical complexity of multi-source Earth observation need not reduce efficiency. By decoupling, sensor-specific physics is handled in lightweight perception modules, while core generative computation is unified in a shared backbone. This preserves cross-modality physical consistency and turns fragmented adaptation into a more homogeneous workload. It also supports interdisciplinary collaboration: domain scientists define constraints and objectives, while computer scientists optimize the shared computational substrate on which these constraints are expressed and enforced.

Finally, the broader significance of this work may extend beyond Earth observation. We do not expect this paradigm to apply uniformly to all scientific data. However, it is likely to be most valuable in domains with four properties: repeated observation of the same or closely related physical system, very large data volume, strong structural redundancy across time or instruments, and downstream use patterns that rarely require unrestricted access to the entire raw archive at full fidelity. Earth observation is an especially strong instance of this regime, but similar opportunities may emerge in other scientific settings such as large sky surveys, climate and environmental monitoring systems, long-horizon simulation archives, and certain high-throughput imaging workflows.

In fact, several large scientific infrastructures are already moving toward science-ready products, regional access centers, and next-to-data analysis rather than unrestricted raw-data distribution to every end user. From this perspective, historical-prior generative compression should be viewed not only as a new Earth observation technique, but as a candidate systems paradigm for future scientific data infrastructures.

In summary, this work points toward a new scientific computing pathway in which historical data are no longer treated merely as stored records, but as executable prior knowledge. By trading large-scale ground computation and long-term learned priors for bandwidth, storage, and data movement, the proposed space-ground collaborative infrastructure opens a practical route toward more efficient, more scalable, and more democratic use of Earth observation data. If sustained and generalized, this paradigm could help redefine not only how remote sensing data are compressed, but how major scientific data systems are acquired, distributed, and ultimately used.

References

- [1] Johannes Ballé, David Minnen, Saurabh Singh, Sung Jin Hwang, and Nick Johnston. 2018. Variational image compression with a scale hyperprior. *arXiv preprint arXiv:1802.01436* (2018).
- [2] Hanbo Bi, Yingchao Feng, Boyuan Tong, Mengyu Wang, Haichen Yu, Yongqiang Mao, Hao Chang, Wenhui Diao, Peijin Wang, Yue Yu, et al. 2025. RingMoE: Mixture-of-modality-experts multi-modal foundation models for universal remote sensing image interpretation. *IEEE Transactions on Pattern Analysis and Machine Intelligence* (2025).
- [3] Mingmin Chi, Antonio Plaza, Jon Atli Benediktsson, Zhongyi Sun, Jinsheng Shen, and Yangyong Zhu. 2016. Big data for remote sensing: Challenges and opportunities. *Proc. IEEE* 104, 11 (2016), 2207–2219.
- [4] Consultative Committee for Space Data Systems. 2005. *Image data compression*. Recommended Standard CCSDS 122.0-B-1. CCSDS. <https://ccsds.org/Pubs/122x0b1c3s.pdf>
- [5] Sajal Dash, Isaac R Lyngaas, Junqi Yin, Xiao Wang, Romain Egele, J Austin Ellis, Matthias Maiterth, Guojing Cong, Feiyi Wang, and Prasanna Balaprakash. 2024. Optimizing distributed training on frontier for large language models. In

- ISC High Performance 2024 Research Paper Proceedings (39th International Conference), Prometheus GmbH, 1–11.
- [6] Gautham Dharuman, Kyle Hippe, Alexander Brace, Sam Foreman, Väinö Hatanpää, Varuni K Sastry, Huihuo Zheng, Logan Ward, Servesh Muralidharan, Archit Vasan, et al. 2024. Mprot-dpo: Breaking the exaflops barrier for multimodal protein design workflows with direct preference optimization. In *SC24: International Conference for High Performance Computing, Networking, Storage and Analysis*. IEEE, 1–13.
 - [7] Matthias Drusch, Umberto Del Bello, Sébastien Carlier, Olivier Colin, Veronica Fernandez, Ferran Gascon, Bianca Hoersch, Claudia Isola, Paolo Laberinti, Philippe Martimort, et al. 2012. Sentinel-2: ESA's optical high-resolution mission for GMES operational services. *Remote sensing of Environment* 120 (2012), 25–36.
 - [8] Kuntai Du, Yihua Cheng, Peder Olsen, Shadi Noghabi, and Junchen Jiang. 2025. Earth+: On-board satellite imagery compression leveraging historical earth observations. In *Proceedings of the 30th ACM International Conference on Architectural Support for Programming Languages and Operating Systems, Volume 1*. 361–376.
 - [9] European Space Agency. 2026. Earth Month 2026: Recent Highlights from the Sentinel Success Stories. <https://sentinels.copernicus.eu/web/success-stories/-/earth-month-2026-recent-highlights-from-the-sentinel-success-stories>. Accessed: 2026-04-12.
 - [10] Mark Everingham, Luc Van Gool, Christopher KI Williams, John Winn, and Andrew Zisserman. 2010. The pascal visual object classes (voc) challenge. *International journal of computer vision* 88, 2 (2010), 303–338.
 - [11] Jorge González-Conejero, Joan Bartrina-Rapesta, and Joan Serra-Sagrata. 2009. JPEG2000 encoding of remote sensing multispectral images with no-data regions. *IEEE Geoscience and Remote Sensing Letters* 7, 2 (2009), 251–255. <https://doi.org/10.1109/LGRS.2009.2032370>
 - [12] Kaiming He, Xiangyu Zhang, Shaoqing Ren, and Jian Sun. 2016. Deep residual learning for image recognition. In *Proceedings of the IEEE conference on computer vision and pattern recognition*. 770–778. <https://doi.org/10.1109/CVPR.2016.90>
 - [13] Henry Herzog, Favien Bastani, Yawen Zhang, Gabriel Tseng, Joseph Redmon, Hadrien Sablon, Ryan Park, Jacob Morrison, Alexandra Buraczynski, Karen Farley, et al. 2025. OlmoEarth: Stable Latent Image Modeling for Multimodal Earth Observation. *arXiv preprint arXiv:2511.13655* (2025).
 - [14] Danfeng Hong, Bing Zhang, Xuyang Li, Yuxuan Li, Chenyu Li, Jing Yao, Naoto Yokoya, Hao Li, Pedram Ghamisi, Xiuping Jia, et al. 2024. SpectralGPT: Spectral remote sensing foundation model. *IEEE transactions on pattern analysis and machine intelligence* 46, 8 (2024), 5227–5244.
 - [15] Johannes Jakubik, Felix Yang, Benedikt Blumenstiel, Erik Scheurer, Rocco Sedona, Stefano Maurogiovanni, Jente Bosmans, Nikolaos Dionelis, Valerio Marsocci, Niklas Kopp, et al. 2025. Terramind: Large-scale generative multimodality for earth observation. In *Proceedings of the IEEE/CVF International Conference on Computer Vision*. 7383–7394.
 - [16] Wei Jiang, Jiayu Yang, Yongqi Zhai, Feng Gao, and Ronggang Wang. 2025. MLC++: Linear complexity multi-reference entropy modeling for learned image compression. *ACM Transactions on Multimedia Computing, Communications and Applications* 21, 5 (2025), 1–25. <https://doi.org/10.1145/3719011>
 - [17] Ziheng Jiang, Haibin Lin, Yinmin Zhong, Qi Huang, Yangrui Chen, Zhi Zhang, Yanghua Peng, Xiang Li, Cong Xie, Shibiao Nong, et al. 2024. {MegaScale}: Scaling large language model training to more than 10,000 {GPU}s. In *21st USENIX Symposium on Networked Systems Design and Implementation (NSDI 24)*. 745–760.
 - [18] Aybora Köksal and A Aydın Alatan. 2025. Tinyrs-r1: Compact vision language model for remote sensing. *IEEE Geoscience and Remote Sensing Letters* (2025).
 - [19] Theodoros Kouzelis, Ioannis Kakogeorgiou, Spyros Gidaris, and Nikos Komodakis. 2025. Eq-vae: Equivariance regularized latent space for improved generative image modeling. *arXiv preprint arXiv:2502.09509* (2025). <https://doi.org/10.48550/arXiv.2502.09509>
 - [20] Hai Li, Yongjun Li, Yuanhao Liu, Boyu Deng, Yu Li, Xin Li, and Shanghong Zhao. 2024. Earth Observation Satellite Downlink Scheduling With Satellite-Ground Optical Communication Links. *IEEE Trans. Aerospace Electron. Systems* 61, 2 (2024), 2281–2294.
 - [21] Yaron Lipman, Ricky TQ Chen, Heli Ben-Hamu, Maximilian Nickel, and Matt Le. 2022. Flow matching for generative modeling. *arXiv preprint arXiv:2210.02747* (2022).
 - [22] Chenyang Liu, Keyan Chen, Rui Zhao, Zhengxia Zou, and Zhenwei Shi. 2025. Text2Earth: Unlocking text-driven remote sensing image generation with a global-scale dataset and a foundation model. *IEEE Geoscience and Remote Sensing Magazine* (2025).
 - [23] Jinming Liu, Heming Sun, and Jiro Katto. 2023. Learned image compression with mixed transformer-cnn architectures. In *Proceedings of the IEEE/CVF conference on computer vision and pattern recognition*. 14388–14397. <https://doi.org/10.1109/CVPR52729.2023.01383>
 - [24] Fabian Mentzer, George D Toderici, Michael Tschannen, and Eirikur Agustsson. 2020. High-fidelity generative image compression. *Advances in neural information processing systems* 33 (2020), 11913–11924. <https://doi.org/10.48550/arXiv.2006.09965>
 - [25] David Minnen, Johannes Ballé, and George D Toderici. 2018. Joint autoregressive and hierarchical priors for learned image compression. In *Advances in Neural Information Processing Systems*, Vol. 31. <https://doi.org/10.48550/arXiv.1809.02736>
 - [26] Deepak Narayanan, Mohammad Shoeybi, Jared Casper, Patrick LeGresley, Mostofa Patwary, Vijay Korthikanti, Dmitri Vainbrand, Prethvi Kashinkunti, Julie Bernauer, Bryan Catanzaro, et al. 2021. Efficient large-scale language model training on gpu clusters using megatron-lm. In *Proceedings of the international conference for high performance computing, networking, storage and analysis*. 1–15.
 - [27] NASA Earthdata. 2025. EOSDIS Annual Metrics. <https://www.earthdata.nasa.gov/about/data-metrics>. Accessed: 2026-04-12.
 - [28] Miloš Radosavljević, Branko Brkjač, Predrag Lugonja, Vladimir Crnojević, Željko Trpovski, Zixiang Xiong, and Dejan Vukobratović. 2020. Lossy compression of multispectral satellite images with application to crop thematic mapping: A HEVC comparative study. *Remote Sensing* 12, 10 (2020), 1590. <https://doi.org/10.3390/rs12101590>
 - [29] Jeff Rasley, Samyam Rajbhandari, Olatunji Ruwase, and Yuxiong He. 2020. DeepSpeed: System optimizations enable training deep learning models with over 100 billion parameters. In *Proceedings of the 26th ACM SIGKDD international conference on knowledge discovery & data mining*. 3505–3506.
 - [30] Philipp Seltsam, Priyanka Das, and Mathias Wien. 2023. Adaptive and scalable compression of multispectral images using VVC. *arXiv preprint arXiv:2301.04117* (2023). <https://doi.org/10.1109/DCC55655.2023.00062>
 - [31] Mohammad Shoeybi, Mostofa Patwary, Raul Puri, Patrick LeGresley, Jared Casper, and Bryan Catanzaro. 2019. Megatron-lm: Training multi-billion parameter language models using model parallelism. *arXiv preprint arXiv:1909.08053* (2019).
 - [32] Siddharth Singh and Abhinav Bhatel. 2022. AxoNN: An asynchronous, message-driven parallel framework for extreme-scale deep learning. In *2022 IEEE International Parallel and Distributed Processing Symposium (IPDPS)*. IEEE, 606–616.
 - [33] Siddharth Singh, Prajwal Singhanian, Aditya Ranjan, John Kirchenbauer, Jonas Geiping, Yuxin Wen, Neel Jain, Abhimanyu Hans, Manli Shu, Aditya Tomar, et al. 2024. Democratizing ai: Open-source scalable llm training on gpu-based supercomputers. In *SC24: International Conference for High Performance Computing, Networking, Storage and Analysis*. IEEE, 1–14.
 - [34] Shaden Smith, Mostofa Patwary, Brandon Norick, Patrick LeGresley, Samyam Rajbhandari, Jared Casper, Zhun Liu, Shrimai Prabhunoye, George Zerveas, Vijay Korthikanti, et al. 2022. Using deepspeed and megatron to train megatron-turing nlg 530b, a large-scale generative language model. *arXiv preprint arXiv:2201.11990* (2022).
 - [35] Marina Sokolova and Guy Lapalme. 2009. A systematic analysis of performance measures for classification tasks. *Information processing & management* 45, 4 (2009), 427–437.
 - [36] Daniela Szwarzman, Sujit Roy, Paolo Fraccaro, Orsteinn Eli Gislason, Benedikt Blumenstiel, Rinki Ghosal, Pedro Henrique De Oliveira, Joao Lucas de Sousa Almeida, Rocco Sedona, Yanghui Kang, et al. 2025. Prithvi-eo-2.0: A versatile multi-temporal foundation model for earth observation applications. *IEEE Transactions on Geoscience and Remote Sensing* (2025).
 - [37] Akihiro Tabuchi, Koichi Shirahata, Masafumi Yamazaki, Akihiko Kasagi, Takumi Honda, Kouji Kurihara, Kentaro Kawakami, Tsuguchika Tabaru, Naoto Fukumoto, Akiyoshi Kuroda, et al. 2021. The 16,384-node parallelism of 3D-CNN training on an arm CPU based supercomputer. In *2021 IEEE 28th International Conference on High Performance Computing, Data, and Analytics (HiPC)*. IEEE, 152–161.
 - [38] Aysim Toker, Lukas Kondmann, Mark Weber, Marvin Eisenberger, Andrés Camero, Jingliang Hu, Ariadna Pregel Hoderlein, Çağlar Senaras, Timothy Davis, Daniel Cremers, Giovanni Marchisio, Xiao Xiang Zhu, and Laura Leal-Taixé. 2022. DynamicEarthNet: Daily Multi-Spectral Satellite Dataset for Semantic Change Segmentation. In *Proceedings of the IEEE/CVF Conference on Computer Vision and Pattern Recognition (CVPR)*. 21158–21167. <https://doi.org/10.1109/CVPR52688.2022.02048>
 - [39] Xiao Wang, Jong-Youl Choi, Takuya Kurihaya, Isaac Lyngaas, Hong-Jun Yoon, Xi Xiao, David Pugmire, Ming Fan, Nasik Muhammad Nafi, Aristeidis Tsaris, et al. 2025. ORBIT-2: Scaling Exascale Vision Foundation Models for Weather and Climate Downscaling. In *Proceedings of the International Conference for High Performance Computing, Networking, Storage and Analysis*. 86–98.
 - [40] Michael A Wulder, Joanne C White, Thomas R Loveland, Curtis E Woodcock, Alan S Belward, Warren B Cohen, Eugene A Fosnight, Jerad Shaw, Jeffrey G Masek, and David P Roy. 2016. The global Landsat archive: Status, consolidation, and direction. *Remote Sensing of Environment* 185 (2016), 271–283.
 - [41] Shao Xiang and Qiaokang Liang. 2024. Remote sensing image compression based on high-frequency and low-frequency components. *IEEE Transactions on Geoscience and Remote Sensing* 62 (2024), 1–15. <https://doi.org/10.1109/TGRS.2023.3349306>

- [42] Zhitong Xiong, Yi Wang, Fahong Zhang, Adam J Stewart, Joëlle Hanna, Damian Borth, Ioannis Papoutsis, Bertrand Le Saux, Gustau Camps-Valls, and Xiao Xiang Zhu. 2024. Neural plasticity-inspired foundation model for observing the earth crossing modalities. *arXiv preprint arXiv:2403.15356* 3, 5 (2024), 6.
- [43] Ruihan Yang and Stephan Mandt. 2023. Lossy image compression with conditional diffusion models. *Advances in Neural Information Processing Systems* 36 (2023), 64971–64995. <https://doi.org/10.48550/arXiv.2209.06950>
- [44] Yixuan Ye, Ce Wang, Wanjie Sun, and Zhenzhong Chen. 2025. Map-Assisted remote-sensing image compression at extremely low bitrates. *ISPRS Journal of Photogrammetry and Remote Sensing* 223 (2025), 159–172. <https://doi.org/10.1016/j.isprsjprs.2025.03.005>
- [45] Guoxia Yu, Tanya Vladimirova, and Martin N Sweeting. 2009. Image compression systems on board satellites. *Acta Astronautica* 64, 9-10 (2009), 988–1005.
- [46] Zhiping Yu, Chenyang Liu, Liqin Liu, Zhenwei Shi, and Zhengxia Zou. 2024. Metaearth: A generative foundation model for global-scale remote sensing image generation. *IEEE Transactions on Pattern Analysis and Machine Intelligence* 47, 3 (2024), 1764–1781.
- [47] Min-Ling Zhang and Zhi-Hua Zhou. 2013. A review on multi-label learning algorithms. *IEEE transactions on knowledge and data engineering* 26, 8 (2013), 1819–1837.
- [48] Yingying Zhang, Lixiang Ru, Kang Wu, Lei Yu, Lei Liang, Yansheng Li, and Jingdong Chen. 2025. SkySense V2: A unified foundation model for multi-modal remote sensing. In *Proceedings of the IEEE/CVF International Conference on Computer Vision*. 9136–9146.
- [49] Ziyuan Zhang, Han Qiu, Maosen Zhang, Jun Liu, Bin Chen, Tianwei Zhang, and Hewu Li. 2024. COSMIC: Compress satellite images efficiently via diffusion compensation. In *Advances in Neural Information Processing Systems 37 (NeurIPS 2024)*. 91951–91982. arXiv:2410.01698 [eess.IV] <https://doi.org/10.52202/079017-2918>
- [50] Xiaohua Zhou, Xuezhi Wang, Yuanchun Zhou, Qinghui Lin, Jianhua Zhao, and Xianghai Meng. 2021. Rsims: Large-scale heterogeneous remote sensing images management system. *Remote Sensing* 13, 9 (2021), 1815.